I-INR: Iterative Implicit Neural Representations

Ali Haider[1], Muhammad Salman Ali[1], Maryam Qamar[1], Tahir Khalil[1], Soo Ye Kim[2], Jihyong Oh[3]*, Enzo Tartaglione[4], Sung-Ho Bae[1]*

[1]Kyung Hee University, Republic of Korea
[2]Adobe Research
[3]Chung-Ang University, Republic of Korea
[4]LTCI, Télécom Paris, Institut Polytechnique de Paris, France
{alihaider, salmanali, maryamqamar, tahirkhalil26}@khu.ac.kr, sooyek@adobe.com,
jihyongoh@cau.ac.kr, enzo.tartaglione@telecom-paris.fr, shbae@khu.ac.kr

Abstract

Implicit Neural Representations (INRs) have revolutionized signal processing and computer vision by modeling signals as continuous, differentiable functions parameterized by neural networks. However, INRs are prone to the spectral bias problem, limiting their ability to retain high-frequency information, and often struggle with noise robustness. Motivated by recent trends in iterative refinement processes, we propose Iterative Implicit Neural Representations (I-INRs). This novel plug-and-play framework iteratively refines signal reconstructions to restore high-frequency details, improve noise robustness, and enhance generalization, ultimately delivering superior reconstruction quality. I-INRs integrate seamlessly into existing INR architectures with only a 0.5–2% increase in parameters. During reconstruction, the iterative refinement adds just 0.8–1.6% additional FLOPs over the baseline while delivering a substantial performance boost of up to +2.0 PSNR. Extensive experiments demonstrate that I-INRs consistently outperform WIRE, SIREN, and Gauss across various computer vision tasks, including image fitting, image denoising, and object occupancy prediction.

Code — https://github.com/Optimizer077/I-INR
Extended version — https://arxiv.org/abs/2504.17364

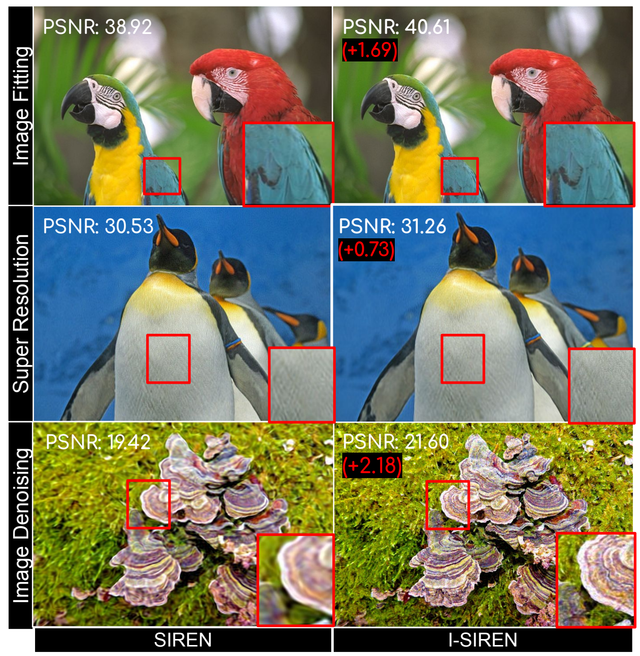

Figure 1: Effectiveness of the proposed methods across multiple tasks, including image fitting, super resolution (2× scale), and denoising, compared to the baseline representative INR method (SIREN). Our novel Iterative-INR method (I-SIREN) consistently improves detail preservation, fidelity, and high-frequency reconstruction across all tasks, outperforming the baseline.

1 Introduction

Implicit Neural Representations (INRs) have emerged as a transformative approach in signal representation, shifting from traditional discrete grid-based methods to continuous coordinate-based models (Sitzmann et al. 2020). By leveraging neural networks, typically multi-layer perceptrons (MLPs), INRs map spatial or temporal coordinates directly to signal attributes such as pixel intensity, colour, or 3D occupancy. This continuous representation inherently offers resolution independence, compact encoding, and seamless interpolation, making INRs highly versatile across a wide range of domains, including computer vision (Chen, Liu, and Wang 2021; Saragadam et al. 2022; Sitzmann et al. 2020; Mildenhall et al. 2021; Jiang, Hua, and Han 2023), and beyond (Sun et al. 2021; Shen et al. 2021; Zhong et al. 2019; Reed et al. 2021). Initially introduced for tasks like 3D shape reconstruction (Mildenhall et al. 2021; Peng et al. 2020; Srinivasan et al. 2021) and novel view synthesis (Irshad et al. 2023), INRs have since been applied to diverse applications including image fitting (Liu et al. 2023b), super-resolution (Delbracio and Milanfar 2023; Saharia et al. 2022), and solving inverse problems (Cha et al. 2024; Wang et al. 2019; Chen, Liu, and Wang 2021).

Despite advancements, INRs continue to face substantial challenges in capturing high-frequency details, maintaining robustness against noise, and handling incomplete

*Corresponding Authors

data (Saragadam et al. 2023). Typically optimized with L1 or L2 loss (Sitzmann et al. 2020), INRs inherently exhibit a spectral bias that favors low-frequency components, often at the expense of fine-grained details (Rahaman et al. 2019).

To mitigate this, recent approaches have introduced positional encoding schemes (Tancik et al. 2020; Fathony et al. 2020) and alternative activation functions (Sitzmann et al. 2020; Saragadam et al. 2023; Liu et al. 2023b; Gao and Jaiman 2024; Thennakoon et al. 2025) to better capture high-frequency content. Positional encodings inject high-frequency signals through orthogonal Fourier bases (Tancik et al. 2020), while periodic activations such as sine functions enable MLPs to model high-frequency structures more effectively compared to traditional ReLU-based networks (Sitzmann et al. 2020). Nevertheless, these methods often assume clean and fully observed inputs, limiting their effectiveness in practical scenarios characterized by noise and occlusion (Saragadam et al. 2023). More recent efforts, such as the integration of complex Gabor wavelet activations, have aimed to improve robustness under such conditions (Saragadam et al. 2023), but challenges persist when scaling to real-world, noisy data. Consequently, there remains significant potential to enhance the fidelity, robustness, and generalization of INRs, particularly in preserving high-frequency signals under adverse conditions.

To address these limitations, and drawing inspiration from iterative models (Delbracio and Milanfar 2023; Rissanen, Heinonen, and Solin 2022; Ho, Jain, and Abbeel 2020), we introduce *Iterative Implicit Neural Representations (I-INRs)* a plug-and-play framework that integrates seamlessly with existing implicit architectures. Unlike traditional single-shot INRs, I-INRs reconstruct signals progressively over multiple iterations, refining details, enhancing reconstruction quality, and improving noise robustness, as illustrated in Figure 1.

The proposed framework features a novel architecture that incorporates existing implicit networks as a BackboneNet without major modifications, while introducing two lightweight modules, i.e FeedbackNet and FuseNet as shown in Figure 2a. These blocks add only 0.5–2% to the total parameter count of the baseline model and support the iterative reconstruction process. Owing to this design, the iterative I-INR process incurs only 0.8–2% additional FLOPs over the baseline INR for two-step reconstruction. Our experiments demonstrate that I-INRs deliver superior reconstructions with enhanced detail, better generalization, and minimal computational overhead, consistently outperforming single-shot methods such as WIRE (Saragadam et al. 2023), SIREN (Sitzmann et al. 2020), and Gauss (Ramasinghe and Lucey 2022) across tasks including image fitting, super-resolution, denoising, and 3D occupancy reconstruction.

Our main contributions are as follows:

- We present **I**terative **I**mplicit **N**eural **R**epresentations, called **I-INRs**, a novel framework for INRs that reconstructs signals *iteratively*, effectively capturing high-frequency details, enhancing robustness to noise, and improving generalization.
- I-INRs are designed as a plug-and-play framework, compatible with existing implicit architectures, enabling seamless integration and adoption in various applications.
- We validate the effectiveness of I-INRs through extensive experiments across multiple tasks, demonstrating superior performance over traditional single-shot INRs in terms of detail reconstruction and robustness.

2 Related Work

Spatial Encoding Techniques. INRs suffer from spectral bias (Rahaman et al. 2019; Tancik et al. 2020), struggling to capture high-fidelity details of complex signals. This limitation affects applications requiring fine-grained detail, such as a single image super resolution (SR), 3D reconstruction, and scene modeling. To address this challenge, various approaches have been proposed, including spatial encoding with frequency-based representations, polynomial decomposition (Raghavan et al. 2023; Singh, Shukla, and Turaga 2023), and high-pass filtering (Fathony et al. 2020), all of which emphasize high-frequency components. DINER (Xie et al. 2023) applies a hash map to unevenly map input coordinates to feature vectors, optimizing spatial frequency distribution for faster, more accurate reconstructions.

Role of Activations. Beyond encoding, activation functions critically influence spectral bias. Standard choices like ReLU cannot capture high-frequency components due to limited representational capacity (Sitzmann et al. 2020). To address this, alternatives such as sinusoidal (Sitzmann et al. 2020) and Gaussian (Ramasinghe and Lucey 2022) activations have been proposed. Activations tuned for high accuracy can suffer from reduced noise robustness; WIRE (Saragadam et al. 2023) leverages Gabor wavelets to provide enhanced robustness to noise. However, there remains room for improvement in achieving both high-frequency fitting and noise robustness (Saragadam et al. 2023).

Iterative Methods. Iterative models have been very successful in image restoration and translation (Saharia et al. 2022; Rissanen, Heinonen, and Solin 2022; Delbracio and Milanfar 2023; Hui et al. 2024; Chu et al. 2025; Chen et al. 2024), video generation (Ji et al. 2025), language modeling (Nie et al. 2025), 3D generation (Qian et al. 2023; Liu et al. 2023a), and more. In contrast with single-shot models, iterative models such as diffusion models (Ho, Jain, and Abbeel 2020; Rissanen, Heinonen, and Solin 2022; Delbracio and Milanfar 2023) produce high-quality samples by reversing degradation processes over multiple steps. Despite their widespread adoption and effectiveness, iterative models remain underexplored in the context of implicit neural representations.

Inspired by the strong detail reconstruction capabilities of iterative models, we propose a novel INR framework that reconstructs signals implicitly over multiple steps. Our approach provides improved details and enhanced noise robustness, offering a flexible, plug-and-play solution that can be integrated into any existing INR framework. However, for the scope of this paper, we specifically focus on

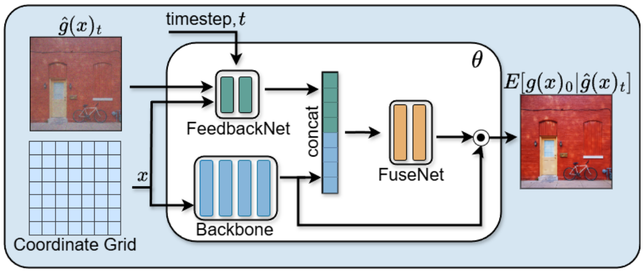

(a)

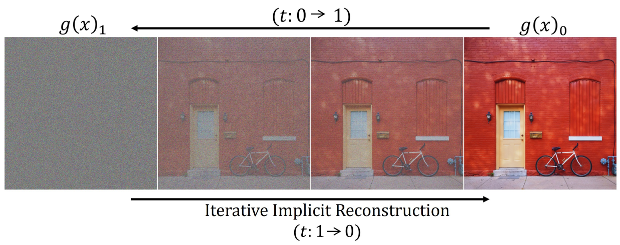

(b)

Figure 2: (a) The proposed architecture of the I-INR model. The framework consists of a Backbone, which can be any baseline INR architecture. Additionally, FeedbackNet incorporates feedback to refine representations, while FuseNet integrates features. The final output is obtained by combining the outputs of the Backbone and the FuseNet, enhancing expressivity and reconstruction quality. (b) Iterative reconstruction process of the proposed I-INR framework.

WIRE (Saragadam et al. 2023), Gauss (Ramasinghe and Lucey 2022), and SIREN (Sitzmann et al. 2020).

3 Preliminary

3.1 Standard INR

Let $g : X \subseteq \mathbb{R}^p \to Y \subseteq \mathbb{R}^q$ be a target function mapping p-dimensional inputs (such as pixel positions in a 2D image or volumetric domains in 3D scenes) to q-dimensional outputs (such as color or density values), such that $y = g(x)$ for $x \in X$. An INR (Sitzmann et al. 2020) is a learnable neural function $f_\theta : X \to Y$, parameterized by θ, aiming to approximate $\mathcal{I}(x)$ across X. The objective is to find θ such that:

$$f_\theta(x) \approx \mathcal{I}(x), \tag{1}$$

where $\mathcal{I}(x)$ represents a true image function evaluated at coordinates x. A typical INR is trained by reducing the signal error in an L_p metric:

$$\min_\theta \mathbb{E}_x \left[\|f_\theta(x) - \mathcal{I}(x)\|_p\right] \approx \min_\theta \sum_i \|f_\theta(x^i) - \mathcal{I}(x^i)\|_p, \tag{2}$$

where $p = 2$ for standard INR training, corresponding to the mean squared error.

3.2 Inversion by Direct Iteration (InDI)

Inversion by Direct Iteration (InDI) (Delbracio and Milanfar 2023) addresses ill-posed inverse problems, such as image restoration, by iteratively refining an estimate of the unknown signal b from an observed measurement a. Instead of solving the full inverse problem in one step, InDI interpolates between a and b via $b_t = ta + (1-t)b$, with $t \in [0, 1]$, and uses a neural network F_θ to approximate the conditional expectation $\mathbb{E}[b \mid b_t]$. The network is trained to minimize:

$$\min_\theta \mathbb{E}_{a,b,t,n} \left[\|F_\theta(b_t + \epsilon_t n,\, t) - b\|_1\right],$$

where $\epsilon_t n$ is Gaussian noise. In inference, the estimate is updated recursively using the learned conditional mean, gradually solving a sequence of easier inverse problems from a to b.

4 Proposed Method

In this section, we present a detailed explanation of our proposed methods, including a comprehensive description of the iterative plug-and-play framework.

4.1 Iterative Implicit Neural Representations: I-INR

I-INR reconstructs the signal over multiple steps, progressively improving the quality at each iteration. As shown in Figure 2b, the process starts from an initial state $g(x)_1 = \mathcal{Z}$ at $t = 1$ and gradually approaches the final reconstruction $g(x)_0 = \mathcal{I}(x)$ at $t = 0$, using steps of size δ. This is achieved by inverting the forward process:

$$g(x)_t = \mathcal{I}(x)(1-t) + \mathcal{Z}t, \qquad t \in [0, 1], \tag{3}$$

where $\mathcal{Z}$ is sampled from a known distribution matching the shape of $\mathcal{I}(x)$.

At each step, I-INR estimates the next state by computing the conditional expectation $\mathbb{E}[g(x)_0 \mid g(x)_t]$, which represents the best possible prediction of the original signal given the current state. This estimate is then used to update the reconstruction as follows:

$$\begin{aligned} \hat{g}(x)_{t-\delta} &= \mathbb{E}\left[g(x)_{t-\delta} \mid \hat{g}(x)_t\right] \\ &= \frac{\delta}{t}\,\mathbb{E}\left[g(x)_0 \mid \hat{g}(x)_t\right] + \left(1 - \frac{\delta}{t}\right)\hat{g}(x)_t, \end{aligned} \tag{4}$$

by repeatedly applying this update, I-INR smoothly transitions from the initial state to the reconstructed signal, leveraging the conditional expectation at each step to improve accuracy.

I–INR Training. To realize the update rule in Eq. (4), we train an implicit neural network f_θ (see Figure. 2a) that maps the intermediate state $\tilde{g}(x)_t$, the spatial coordinates x, and the time index t directly to the clean target $\mathcal{I}(x)$:

$$\min_\theta \; \mathbb{E}_{x,\,t,\,n} \left\| f_\theta\big(\tilde{g}(x)_t,\, x,\, t\big) - \mathcal{I}(x) \right\|_2^2, \tag{5}$$

$$\tilde{g}(x)_t = (1-t)\,\mathcal{I}(x) + t\,\mathcal{Z} + \varepsilon t n, \tag{6}$$

where $\mathcal{Z} \sim p(\mathcal{Z})$ and $n \sim \mathcal{N}(0, 1)$. The small perturbation $\varepsilon t n$ (Delbracio and Milanfar 2023) satisfies the regularity requirement, guaranteeing stable reconstruction during inference. The full training procedure appears in Algorithm 1.

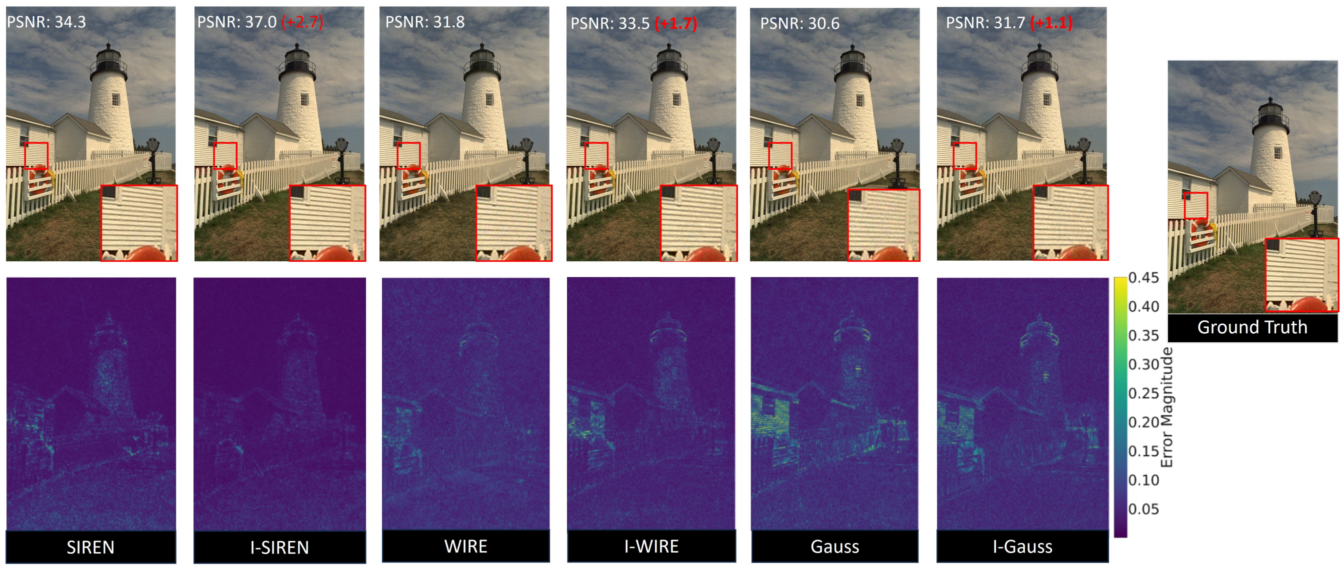

Figure 3: Image fitting results for different non-linearities and their iterative extensions (prefix ”I”). Each column presents the reconstructed image (top) and residual map (bottom), highlighting reconstruction quality. PSNR values are reported, with iterative improvements in red. The rightmost column shows the ground truth.

I–INR Reconstruction. Reconstruction begins from the latent state $\mathcal{Z}$ and proceeds for $1/\delta$ iterations of Eq. 4, iteratively refining the estimate towards the final signal (Algorithm 2).

Algorithm 1: I-INRs Model Training of f_θ

Require: $\mathcal{I}(x)$, ε, η

$\mathcal{Z} \sim p(\mathcal{Z})$
repeat
  $x \sim p(x)$
  $t \sim \mathcal{U}(0,1),\ n \sim \mathcal{N}(0,I)$
  $\tilde{g}(x)_t \leftarrow (1-t)\,\mathcal{I}(x) + t\,\mathcal{Z} + \varepsilon\, t\, n$
  $\theta \leftarrow \theta - \eta\,\nabla_\theta \big\| f_\theta(\tilde{g}(x)_t,\, x,\, t) - \mathcal{I}(x) \big\|_2^2$
until converged

Algorithm 2: I-INRs Model Reconstruction

Require: $\mathcal{Z}$, f_θ, δ, x

$\hat{g}(x)_1 \leftarrow \mathcal{Z}$
for $t \leftarrow 1$ **to** 0 **step** $-\delta$ **do**
  $\hat{g}(x)_{t-\delta} \leftarrow \dfrac{\delta}{t}\, f_\theta\big(\hat{g}(x)_t, x, t\big) + \left(1 - \dfrac{\delta}{t}\right) \hat{g}(x)_t$
end for
return $\hat{g}(x)_0$

Network Architecture. Figure 2a provides an overview of our plug-and-play I-INR framework, which comprises three main components: a Backbone network, a FeedbackNet module, and a FuseNet module. The Backbone extracts initial features from the input; the FeedbackNet incorporates the intermediate state and time conditioning; and the FuseNet merges these feature streams. The final output is given by Eq. (7). This design enables flexible integration with existing INR architectures and supports efficient iterative refinement. The information flow between components is formalized as

$$f_\theta\big(\hat{g}(x)_t,\, x,\, t\big) = \mathrm{FuseNet}\big(\mathrm{concat}(\mathbf{f}, \mathbf{b})\big) \odot \mathbf{b}, \qquad (7)$$

where

$$\mathbf{b} := \mathrm{Backbone}(x), \qquad \mathbf{f} := \mathrm{FeedbackNet}\big(\hat{g}(x)_t,\, x,\, t\big).$$

At each iteration, the current state is processed by the FeedbackNet, and its output is fused with the Backbone features via FuseNet. Notably, the Backbone is forward-passed only once throughout the reconstruction, while the lightweight FeedbackNet and FuseNet operate at each iteration, resulting in a substantial reduction in computational cost.

5 Experiments

To evaluate the effectiveness and robustness of our proposed method, we conduct extensive experiments across diverse tasks and backbones. Our evaluation encompasses regression tasks, such as 2D and 3D signal fitting, as well as generalization and robustness tasks, including image SR and image denoising. To demonstrate its comparative advantage, we benchmark our method against established baseline approaches, including SIREN, Gauss, and WIRE.

Implementation Settings. The proposed I-INR framework is implemented in PyTorch (Paszke et al. 2019) and optimized using the Adam optimizer (Diederik 2014). For all experiments, the noise parameter ϵ is empirically set to 0.1, and the inference *steps* are fixed to 2 unless stated otherwise. The initial state $\mathcal{Z}$ is sampled from a standard normal Gaussian distribution across all experiments. All baseline

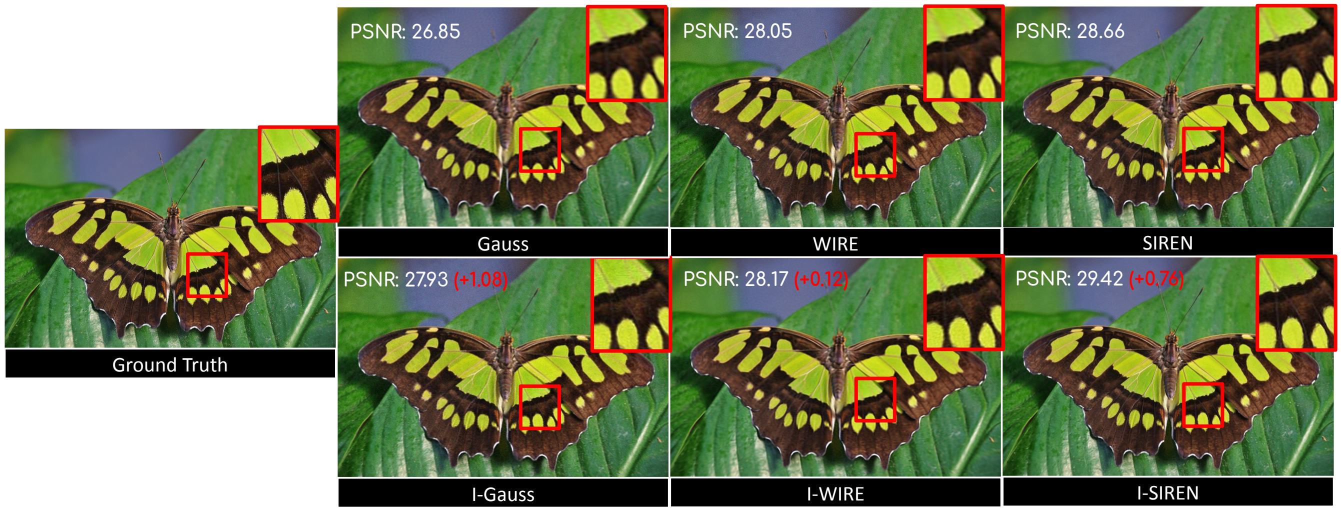

Figure 4: Visual quality comparison of super-resolution results at 2× scale using various methods. The ground truth is compared against baseline INR methods SIREN, WIRE, Gauss, and their iterative counterparts. The iterative approaches consistently achieve sharper reconstructions with fewer artifacts, effectively preserving finer details and high-frequency structures.

	SIREN		**WIRE**		**Gauss**	
	PSNR ↑	SSIM ↑	PSNR ↑	SSIM ↑	PSNR ↑	SSIM ↑
Baseline	34.57	0.931	32.15	0.898	31.33	0.880
Ours	**37.53**	**0.961**	**33.73**	**0.924**	**31.93**	**0.884**

Table 1: Image fitting results on Kodak comparing SIREN, WIRE, and Gauss with their iterative counterparts.

Scale	**Method**	**SIREN**		**WIRE**		**Gauss**	
		PSNR ↑	LPIPS ↓	PSNR ↑	LPIPS ↓	PSNR ↑	LPIPS ↓
2×	Baseline	26.77	0.414	26.14	0.457	25.19	0.538
	Ours	**27.64**	**0.367**	**27.21**	**0.388**	**26.82**	**0.363**
4×	Baseline	25.03	0.597	24.57	0.618	23.85	0.673
	Ours	**25.53**	**0.575**	**25.78**	**0.496**	**25.18**	**0.620**

Table 2: Comparison of (SR) performance for 2× and 4× upscaling using a model trained on 2× SR. Results are shown alongside SIREN, WIRE, and Gauss, including their iterative counterparts. The best results are shown in bold.

methods, including SIREN, WIRE, and Gauss, as well as their iterative counterparts, are initialized following the configurations specified in their respective papers. In our implementation, both FeedbackNet and FuseNet are lightweight MLPs with two layers, each layer having a width of 30 for FeedbackNet and 100 for FuseNet.

Evaluation Metrics. To comprehensively evaluate our proposed method, we conduct extensive experiments using both distortion-based metrics, such as Peak Signal-to-Noise Ratio (PSNR) and Structural Similarity Index Measure (SSIM) (Wang et al. 2004), as well as perceptual metrics like Learned Perceptual Image Patch Similarity (LPIPS) (Zhang et al. 2018).

5.1 Results

Our results consistently demonstrate that I-INR outperforms existing methods across diverse tasks, including image fitting, SR, and 3D occupancy. It achieves superior reconstruction quality and enhanced robustness compared to baseline approaches (SIREN, WIRE, Gauss).

Image Fitting. For image fitting, each baseline employs a 3-layer MLP with 300 neurons per layer, serving as the Backbone INR for iterative models (Figure 2a). All networks are trained on the full-resolution Kodak dataset (Kodak 1993), with average results reported in Table 1. The proposed iterative models consistently outperform their one-shot counterparts. As shown in Figure 3, error maps from baseline models display uniform noise, especially in high-frequency regions, whereas iterative variants produce smoother reconstructions with reduced errors, including in challenging areas.

Image Super-resolution. We evaluate our I-INR framework against traditional one-shot INRs on SR tasks using 40 images from the DIV2K dataset (Agustsson and Timofte 2017). The model is trained exclusively on 2× SR with a two-layer MLP of 256 neurons per layer. To assess generalization, we evaluate I-INR on both 2× and 4× SR, despite training only on 2×. Table 2 compares its performance with single-shot baselines, demonstrating that our approach consistently enhances fidelity (PSNR) and perceptual quality (LPIPS) across all architectures. Figure 4 visualizes the butterfly image for 2× SR, comparing each baseline with its iterative counterpart. The proposed approach consistently outperforms baseline methods, generating sharper reconstructions with fewer artifacts across all non-linearities.

Image Denoising. To assess the robustness of I-INRs in modeling noisy signals, we utilize 40 high-resolution color images from the DIV2K dataset and introduce Poisson-

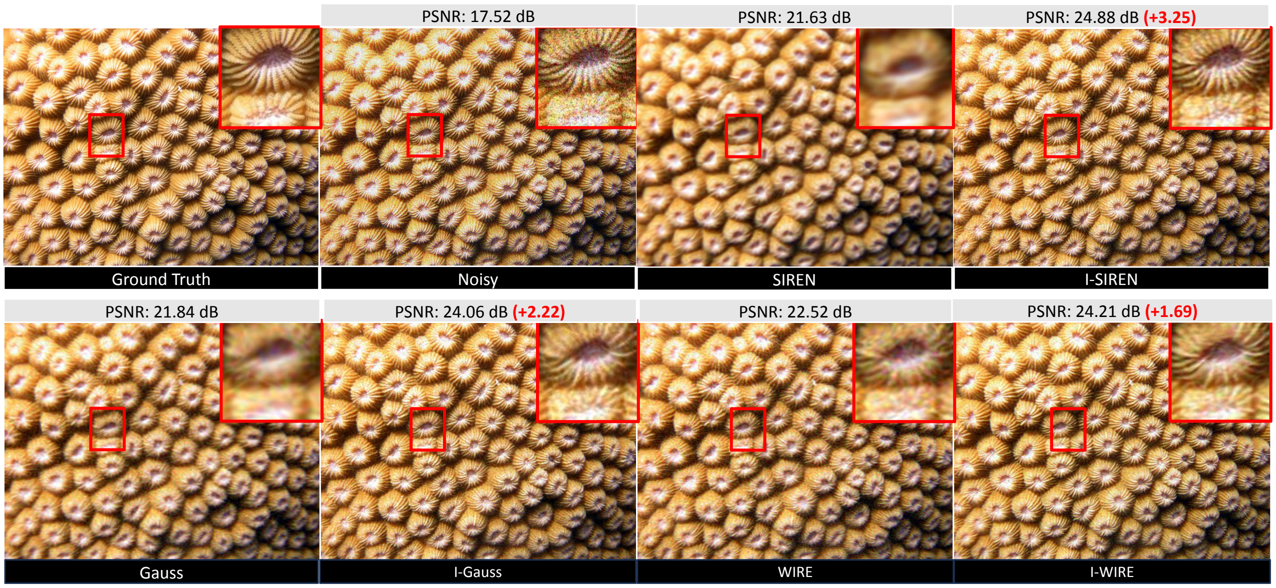

Figure 5: Visual comparison of denoising results using various methods. The ground truth is compared against noisy input, baseline methods SIREN, WIRE, and Gauss, as well as their iterative counterparts. I-INR demonstrates superior artifact reduction and detail preservation compared to their non-iterative counterparts.

	SIREN		**WIRE**		**Gauss**	
	PSNR ↑	LPIPS ↓	PSNR ↑	LPIPS ↓	PSNR ↑	LPIPS ↓
Baseline	23.86	0.604	23.32	0.746	23.10	0.783
Ours	**25.59**	**0.540**	**24.76**	**0.490**	**24.20**	**0.533**

Table 3: Image denoising results on 40 images sampled from the DIV2K dataset, comparing SIREN, WIRE, and Gauss with their iterative counterparts.

	SIREN ↑	**WIRE ↑**	**Gauss ↑**
Baseline	0.9840	0.9917	0.9855
Ours	**0.9934**	**0.9950**	**0.9967**

Table 4: Averaged Intersection over Union (IoU) results comparing SIREN, WIRE, and Gauss with their iterative counterparts on the Armadillo, Dragon, and Thai Statue 3D.

distributed noise to each pixel, with a maximum mean photon count of 30 and a readout noise level of 2, following (Saragadam et al. 2023). The same architecture and training procedure as SR is employed. Table 3 presents quantitative results comparing the denoising performance of baseline architectures with their iterative counterparts. Iterative models consistently achieve significant improvements in both PSNR and LPIPS over their single-shot baselines. Figure 5 provides a qualitative comparison of denoising performance for SIREN, WIRE, and Gauss alongside their iterative versions. The iterative approach significantly enhances reconstruction quality across all architectures, achieving up to +3.25 dB PSNR improvement (for SIREN).

3D Occupancy. The 3D occupancy task aims to reconstruct 3D shapes by modeling the occupancy of points in space. We conduct experiments on the Armadillo, Dragon, and Thai Statue 3D scenes (Gal and Cohen-Or 2006), utilizing a two-layer MLP with 256 neurons per layer for both the baseline INRs and their iterative counterparts. Table 4 presents the averaged Intersection over Union (IoU) results, while Figure 6 visualizes the reconstructions achieved using different nonlinearities and their iterative variants. Notably, I-INRs outperform their single-shot baselines, generating sharper and more precise reconstructions. The iterative approach enhances detail preservation, particularly in complex regions as shown in Figure 6.

5.2 Ablation Studies

We ablate inference complexity, Feedback/FuseNet impact, and reconstruction steps. Further analysis on initial state, training cost, layer depth, and statistical significance is included in the extended version of the paper.

Inference Complexity. During reconstruction, I-SIREN executes the Backbone network only once, while subsequent refinement steps involve forward passes through the lightweight FeedbackNet and FuseNet modules. The iterative setup introduces minimal computational overhead: the Backbone accounts for 106.8 GFLOPs, and each refinement step adds just 0.43 GFLOPs. For two refinement steps ($\text{steps} = 2$), the total computational cost amounts to 107.6 GFLOPs, approximately equivalent to the original SIREN.

Impact of FeedbackNet and FuseNet: To evaluate the impact of architectural components of I-INR, we performed ablation studies by selectively disabling the FeedbackNet

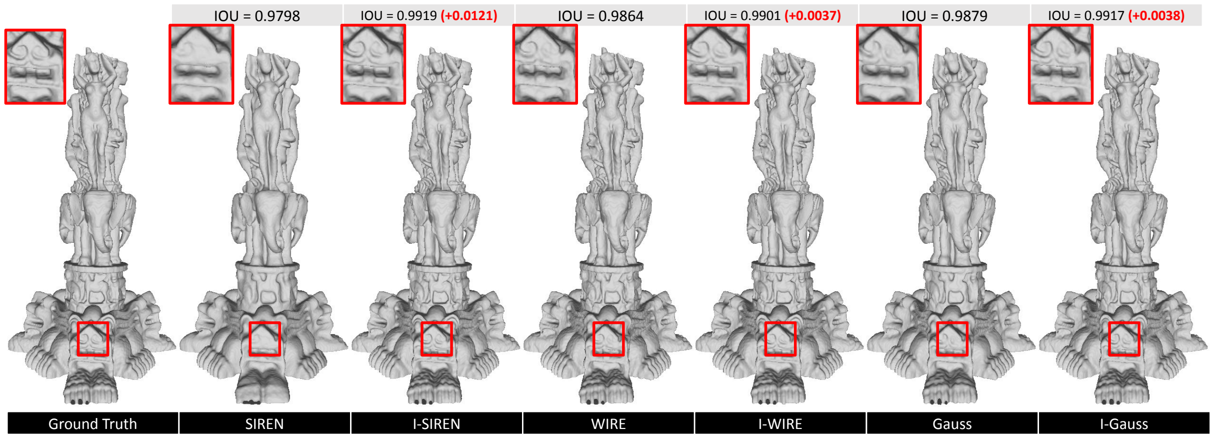

Figure 6: Visualization of 3D occupancy reconstruction results using various methods and their iterative counterparts. The ground truth is compared to baseline models SIREN, WIRE, Gauss, and their iterative counterparts.

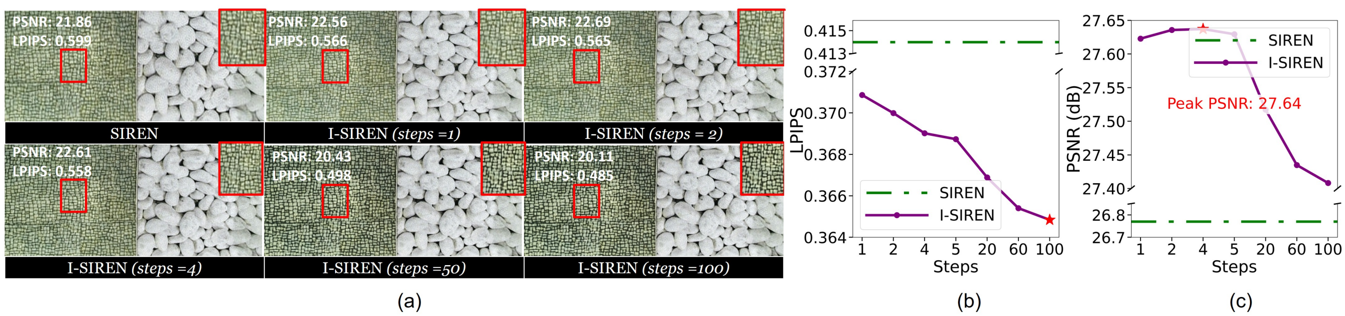

Figure 7: Analysis of I-SIREN's performance for super-resolution at $2\times$ resolution across different iteration $steps$. (a) I-SIREN achieves peak PSNR at $steps = 4$, where further increasing time steps enhances perceptual quality but reduces fidelity due to the fidelity-perception tradeoff. (b) Increasing the number of steps consistently improves perceptual quality. (c) PSNR reaches its highest performance at $steps = 4$, and while additional iterations slightly reduce PSNR, it remains superior to the baseline.

FeedbackNet (Params)	**FuseNet (Params)**	**PSNR**
✗	✗	20.27
✓ ($1\times$)	✗	31.88
✓ ($1\times$)	✓ ($1\times$)	37.53
✓ ($2\times$)	✓ ($1\times$)	37.25
✓ ($1\times$)	✓ ($2\times$)	37.77
✓ ($2\times$)	✓ ($2\times$)	37.56

Table 5: Impact of FeedbackNet and FuseNet on image fitting task with I-SIREN on the Kodak dataset.

and FuseNet modules and varying their parameter scales. These experiments were conducted on the image fitting task using I-SIREN on the Kodak dataset. As summarized in Table 5, removing both modules results in a significant performance drop, with the PSNR falling to 20.27. Introducing FeedbackNet alone substantially improves reconstruction quality, and the addition of FuseNet provides further gains. The best performance is achieved when both modules are included, with moderate parameter scaling yielding an optimal balance between computational cost and accuracy.

Analysis of Reconstruction Steps. We evaluate the effect of reconstruction steps on $2\times$ super-resolution using 40 images from the DIV2K dataset (Figures 7b and 7c). PSNR peaks at $steps = 4$, with the largest improvement from 1 to 2 steps; beyond 2, gains saturate. While PSNR slightly drops for $steps > 4$, perceptual quality (LPIPS) continues to improve, reflecting the Perception-Distortion Tradeoff (Blau and Michaeli 2018). Figure 7a visually compares SIREN and I-SIREN across steps, showing that I-SIREN produces increasingly vivid and detailed reconstructions, confirming that additional refinement steps are beneficial for capturing finer textures and high-frequency components.

6 Conclusion

This work introduces a novel I-INR framework that progressively reconstructs a signal. The proposed method serves as a plug-and-play solution compatible with existing INR methods, significantly enhancing their performance. Through extensive experiments, we demonstrate that I-INR effectively captures high-frequency details, improves noise robustness, and achieves superior reconstruction quality across various tasks and nonlinearities.

Acknowledgments

This work was supported by the National Research Foundation of Korea (NRF) grant funded by the Korea government (MSIT) (No. RS-2025-24534076) and (No. RS-2025-02216217), and by the IITP (Institute of Information & Communications Technology Planning & Evaluation) – ITRC (Information Technology Research Center) grant funded by the Korea government (Ministry of Science and ICT) (IITP-2025-RS-2024-00438239). Part of this work was also funded by Hi!PARIS Center on Data Analytics and Artificial Intelligence.

References

Agustsson, E.; and Timofte, R. 2017. Ntire 2017 challenge on single image super-resolution: Dataset and study. In *Proceedings of the IEEE conference on computer vision and pattern recognition workshops*, 126–135.

Blau, Y.; and Michaeli, T. 2018. The perception-distortion tradeoff. In *Proceedings of the IEEE conference on computer vision and pattern recognition*, 6228–6237.

Cha, J.; Haider, A.; Yang, S.; Jin, H.; Yang, S.; Uddin, A. S.; Kim, J.; Kim, S. Y.; and Bae, S.-H. 2024. Descanning: From scanned to the original images with a color correction diffusion model. In *Proceedings of the AAAI Conference on Artificial Intelligence*, volume 38, 954–963.

Chen, Y.; Liu, S.; and Wang, X. 2021. Learning continuous image representation with local implicit image function. In *Proceedings of the IEEE/CVF conference on computer vision and pattern recognition*, 8628–8638.

Chen, Y.; Wang, O.; Zhang, R.; Shechtman, E.; Wang, X.; and Gharbi, M. 2024. Image neural field diffusion models. In *Proceedings of the IEEE/CVF Conference on Computer Vision and Pattern Recognition*, 8007–8017.

Chu, J.; Du, C.; Lin, X.; Zhang, X.; Wang, L.; Zhang, Y.; and Wei, H. 2025. Highly accelerated MRI via implicit neural representation guided posterior sampling of diffusion models. *Medical Image Analysis*, 100: 103398.

Delbracio, M.; and Milanfar, P. 2023. Inversion by direct iteration: An alternative to denoising diffusion for image restoration. *Transactions on Machine Learning Research*.

Diederik, P. K. 2014. Adam: A method for stochastic optimization. *(No Title)*.

Fathony, R.; Sahu, A. K.; Willmott, D.; and Kolter, J. Z. 2020. Multiplicative filter networks. In *International Conference on Learning Representations*.

Gal, R.; and Cohen-Or, D. 2006. Salient geometric features for partial shape matching and similarity. *ACM Transactions on Graphics (TOG)*, 25(1): 130–150.

Gao, R.; and Jaiman, R. K. 2024. H-SIREN: Improving implicit neural representations with hyperbolic periodic functions. *arXiv preprint arXiv:2410.04716*.

Ho, J.; Jain, A.; and Abbeel, P. 2020. Denoising diffusion probabilistic models. *Advances in neural information processing systems*, 33: 6840–6851.

Hui, M.; Wei, Z.; Zhu, H.; Xia, F.; and Zhou, Y. 2024. Microdiffusion: Implicit representation-guided diffusion for 3D reconstruction from limited 2D microscopy projections. In *Proceedings of the IEEE/CVF Conference on Computer Vision and Pattern Recognition*, 11460–11469.

Irshad, M. Z.; Zakharov, S.; Liu, K.; Guizilini, V.; Kollar, T.; Gaidon, A.; Kira, Z.; and Ambrus, R. 2023. NeO 360: Neural Fields for Sparse View Synthesis of Outdoor Scenes. In *Proceedings of the IEEE/CVF International Conference on Computer Vision (ICCV)*, 9187–9198.

Ji, S.; Luo, H.; Chen, X.; Tu, Y.; Wang, Y.; and Zhao, H. 2025. LayerFlow: A Unified Model for Layer-aware Video Generation. *arXiv preprint arXiv:2506.04228*.

Jiang, S.; Hua, J.; and Han, Z. 2023. Coordinate quantized neural implicit representations for multi-view reconstruction. In *Proceedings of the IEEE/CVF international conference on computer vision*, 18358–18369.

Kodak, E. 1993. Kodak lossless true color image suite (PhotoCD PCD0992).

Liu, R.; Wu, R.; Van Hoorick, B.; Tokmakov, P.; Zakharov, S.; and Vondrick, C. 2023a. Zero-1-to-3: Zero-shot one image to 3d object. In *Proceedings of the IEEE/CVF international conference on computer vision*, 9298–9309.

Liu, Z.; Zhu, H.; Zhang, Q.; Fu, J.; Deng, W.; Ma, Z.; Guo, Y.; and Cao, X. 2023b. FINER: Flexible spectral-bias tuning in Implicit NEural Representation by Variable-periodic Activation Functions. *arXiv preprint arXiv:2312.02434*.

Mildenhall, B.; Srinivasan, P. P.; Tancik, M.; Barron, J. T.; Ramamoorthi, R.; and Ng, R. 2021. Nerf: Representing scenes as neural radiance fields for view synthesis. *Communications of the ACM*, 65(1): 99–106.

Nie, S.; Zhu, F.; You, Z.; Zhang, X.; Ou, J.; Hu, J.; Zhou, J.; Lin, Y.; Wen, J.-R.; and Li, C. 2025. Large language diffusion models. *arXiv preprint arXiv:2502.09992*.

Paszke, A.; Gross, S.; Massa, F.; Lerer, A.; Bradbury, J.; Chanan, G.; Killeen, T.; Lin, Z.; Gimelshein, N.; Antiga, L.; et al. 2019. Pytorch: An imperative style, high-performance deep learning library. *Advances in neural information processing systems*, 32.

Peng, S.; Niemeyer, M.; Mescheder, L.; Pollefeys, M.; and Geiger, A. 2020. Convolutional occupancy networks. In *Computer Vision–ECCV 2020: 16th European Conference, Glasgow, UK, August 23–28, 2020, Proceedings, Part III 16*, 523–540. Springer.

Qian, G.; Mai, J.; Hamdi, A.; Ren, J.; Siarohin, A.; Li, B.; Lee, H.-Y.; Skorokhodov, I.; Wonka, P.; Tulyakov, S.; et al. 2023. Magic123: One image to high-quality 3d object generation using both 2d and 3d diffusion priors. *arXiv preprint arXiv:2306.17843*.

Raghavan, N.; Xiao, Y.; Lin, K.-E.; Sun, T.; Bi, S.; Xu, Z.; Li, T.-M.; and Ramamoorthi, R. 2023. Neural Free-Viewpoint Relighting for Glossy Indirect Illumination. In *Computer Graphics Forum*, volume 42, e14885. Wiley Online Library.

Rahaman, N.; Baratin, A.; Arpit, D.; Draxler, F.; Lin, M.; Hamprecht, F.; Bengio, Y.; and Courville, A. 2019. On the spectral bias of neural networks. In *International conference on machine learning*, 5301–5310. PMLR.

Ramasinghe, S.; and Lucey, S. 2022. Beyond periodicity: Towards a unifying framework for activations in coordinate-mlps. In *European Conference on Computer Vision*, 142–158. Springer.

Reed, A.; Blanford, T.; Brown, D. C.; and Jayasuriya, S. 2021. Implicit neural representations for deconvolving SAS images. In *OCEANS 2021: San Diego–Porto*, 1–7. IEEE.

Rissanen, S.; Heinonen, M.; and Solin, A. 2022. Generative modelling with inverse heat dissipation. *arXiv preprint arXiv:2206.13397*.

Saharia, C.; Ho, J.; Chan, W.; Salimans, T.; Fleet, D. J.; and Norouzi, M. 2022. Image super-resolution via iterative refinement. *IEEE transactions on pattern analysis and machine intelligence*, 45(4): 4713–4726.

Saragadam, V.; LeJeune, D.; Tan, J.; Balakrishnan, G.; Veeraraghavan, A.; and Baraniuk, R. G. 2023. Wire: Wavelet implicit neural representations. In *Proceedings of the IEEE/CVF Conference on Computer Vision and Pattern Recognition*, 18507–18516.

Saragadam, V.; Tan, J.; Balakrishnan, G.; Baraniuk, R. G.; and Veeraraghavan, A. 2022. Miner: Multiscale implicit neural representation. In *European Conference on Computer Vision*, 318–333. Springer.

Shen, S.; Wang, Z.; Liu, P.; Pan, Z.; Li, R.; Gao, T.; Li, S.; and Yu, J. 2021. Non-line-of-sight imaging via neural transient fields. *IEEE Transactions on Pattern Analysis and Machine Intelligence*, 43(7): 2257–2268.

Singh, R.; Shukla, A.; and Turaga, P. 2023. Polynomial implicit neural representations for large diverse datasets. In *Proceedings of the IEEE/CVF Conference on Computer Vision and Pattern Recognition*, 2041–2051.

Sitzmann, V.; Martel, J.; Bergman, A.; Lindell, D.; and Wetzstein, G. 2020. Implicit neural representations with periodic activation functions. *Advances in neural information processing systems*, 33: 7462–7473.

Srinivasan, P. P.; Deng, B.; Zhang, X.; Tancik, M.; Mildenhall, B.; and Barron, J. T. 2021. Nerv: Neural reflectance and visibility fields for relighting and view synthesis. In *Proceedings of the IEEE/CVF Conference on Computer Vision and Pattern Recognition*, 7495–7504.

Sun, Y.; Liu, J.; Xie, M.; Wohlberg, B.; and Kamilov, U. S. 2021. Coil: Coordinate-based internal learning for imaging inverse problems. *arXiv preprint arXiv:2102.05181*.

Tancik, M.; Srinivasan, P.; Mildenhall, B.; Fridovich-Keil, S.; Raghavan, N.; Singhal, U.; Ramamoorthi, R.; Barron, J.; and Ng, R. 2020. Fourier features let networks learn high frequency functions in low dimensional domains. *Advances in neural information processing systems*, 33: 7537–7547.

Thennakoon, P.; Ranasinghe, A.; De Silva, M.; Epakanda, B.; Godaliyadda, R.; Ekanayake, P.; and Herath, V. 2025. BandRC: Band Shifted Raised Cosine Activated Implicit Neural Representations. *arXiv preprint arXiv:2505.11640*.

Wang, T.; Yang, X.; Xu, K.; Chen, S.; Zhang, Q.; and Lau, R. W. 2019. Spatial attentive single-image deraining with a high quality real rain dataset. In *Proceedings of the IEEE/CVF conference on computer vision and pattern recognition*, 12270–12279.

Wang, Z.; Bovik, A. C.; Sheikh, H. R.; and Simoncelli, E. P. 2004. Image quality assessment: from error visibility to structural similarity. *IEEE transactions on image processing*, 13(4): 600–612.

Xie, S.; Zhu, H.; Liu, Z.; Zhang, Q.; Zhou, Y.; Cao, X.; and Ma, Z. 2023. Diner: Disorder-invariant implicit neural representation. In *Proceedings of the IEEE/CVF Conference on Computer Vision and Pattern Recognition*, 6143–6152.

Zhang, R.; Isola, P.; Efros, A. A.; Shechtman, E.; and Wang, O. 2018. The unreasonable effectiveness of deep features as a perceptual metric. In *Proceedings of the IEEE conference on computer vision and pattern recognition*, 586–595.

Zhong, E. D.; Bepler, T.; Davis, J. H.; and Berger, B. 2019. Reconstructing continuous distributions of 3D protein structure from cryo-EM images. *arXiv preprint arXiv:1909.05215*.